Surface Science 289 (1993) 85–99
North-Holland

surface science

Coupling nitrosyls as the first step in the reduction of NO on metal surfaces: the special role of rhodium

Thomas R. Ward [a], Roald Hoffmann [a,*] and Mordecai Shelef [b]

[a] *Department of Chemistry and Material Science Center, Cornell University, Ithaca, NY 14853–1301, USA*
[b] *Research Staff, Ford Motor Company, Dearborn, MI 48121, USA*

Received 16 September 1992; accepted for publication 7 January 1993

The adsorption of NO and its coupling to yield N_2O_2 on Rh(100), Pd(100) and Pt(100) surfaces is analyzed using extended Hückel calculations. It appears that the Blyholder model is a valid description of the chemisorption of NO on Rh(100). There is substantial weakening of the NO bond on this surface. However, in the case of Pd(100) and Pt(100), the N–O overlap population increases upon chemisorption. For some of the geometries studied, the results indicate that for rhodium surfaces the coupled product has significant N–N double bond character, best described by the 6π electron system, hyponitrite. For rhodium surfaces the dimerization of chemisorbed NO seems to be a viable initial step in the NO reduction mechanism.

1. Introduction

The catalytic reduction of nitric oxide over transition-metal surfaces plays a central role in air pollution alleviation. For this purpose, rhodium was introduced into general usage in US automotive catalysts in 1981 to meet the stringent standards for NO_x emissions which went into effect that year. Until that time, catalysts containing platinum and palladium had been used to oxidize CO and hydrocarbons [1]. The characteristic of the three-way catalyst (TWC) is the removal of all three regulated pollutants (HC, CO and NO_x).

The role of rhodium in the TWC has not been fully elucidated as yet, but it is clear that it plays a key function in the NO reduction, outperforming the other components of the TWC. In this regard, the study of rhodium–platinum alloys is instructive. Recent work with $Rh_{0.5}$–$Pt_{0.5}$ alloys clearly indicates that for an NO and CO gas mixture, the CO molecules adsorb preferentially on Pt sites, whereas the NO molecules adsorb primarily on Rh sites [2]. Further, looking at the $NO + CO$ versus $NO + H_2$ reduction rates on various transition-metal surfaces, it has been found that the latter pathway is fastest for both platinum and palladium surfaces, thus producing ammonia rather than dinitrogen. This tendency is reversed for rhodium, iridium and ruthenium surfaces [3].

Nitric oxide chemisorption on transition-metal surfaces has been studied extensively [4–13]. In discrete complexes and on surfaces, the NO ligand may bind linearly or bent. At the molecular level these bonding modes may be described as $M–(NO)^+$ for the linear case, and $M–(NO)^-$ for the bent form [11,14–17]. On surfaces the picture is complicated by the dissociative adsorption of NO. This latter process eventually leads to recombination and desorption of N_2 and O_2. It is generally accepted that NO dissociation is a prerequisite for its efficient reduction over metal surfaces. Since dissociative chemisorption is the trend for group 9 metal surfaces [18–21] but not group 10 surfaces [4,22–26,9], this argument could account for the difference in reactivity between Rh (group 9), Pd and Pt surfaces (group 10). At low coverages, it appears that NO adsorbs mostly on bridging sites for Pd [9,26,27], Pt [28–30] and Rh [31].

* To whom correspondence should be addressed.

Upon increasing the coverage, this picture becomes much more complex. To illustrate this with a single example, we mention the work of Somorjai and coworkers, who reported at least five different NO species on Rh(111) using high-resolution EELS [6]. The presence of pairs of nitrosyls has recurrently been reported for various surfaces [27,32–42]. This geometry, particularly favorable for an N–N coupling, leading to the formation of dinitrogen dioxide, has received relatively little attention. In this respect, one should remember the gas-phase reactions of NO with H_2, CO, SO_2 and O_2. These involve third-order reaction rates, proportional to the square of the nitric oxide concentration, strongly suggesting a nitrosyl–dinitrogen dioxide pre-equilibrium [43]. The presence of such a pre-equilibrium was proposed as early as 1918 by Bodenstein to account for the third-order rate constant for the reaction between NO and O_2 to form NO_2 [44].

The formation of NO dimers has been observed in the condensed phase and in the gas phase. Three different experimental structural determinations for N_2O_2 have been reported [45–48]. The crystal structure of dinitrogen dioxide was resolved crystallographically by Lipscomb [45]. The N–N bond length is unusually long, 2.18 Å. Dinerman and Ewing deduced the structure of gas-phase N_2O_2 by performing contour analyses of two IR bands [46]. In this study, the N–N bond length was found to be 1.75 Å. A second experimental structural determination of N_2O_2 in the gas phase suggests a N–N bond length of 2.33 Å [47]. Several ab initio full geometry optimizations have been performed. At the SCF level of theory, N–N bond distances of 1.7862 [48] and 1.615 Å [49] were obtained. Inclusion of electron correlation leads to an N–N distance of 2.186 Å at the MP2 level of theory [50]. A metastable form of N_2O_2 with an N–N distance of 1.25 Å has been suggested to serve as an important intermediate in the high pressure reaction $2NO \rightarrow N_2 + O_2$ [51].

The presence of a dinitrogen dioxide ligand coordinated to a metal fragment has been reported only on a couple of occasions [52,53]. To our knowledge, two theoretical analyses have been carried out on molecular systems to simulate the coupling of two cis-coordinated nitrosyl ligands on a metal template, leading to a dinitrogen dioxide with a N–N bond. For the tetrahedral complex $[FeCl_2(NO)_2]$, the reaction was predicted to be symmetry allowed [54], as well as for $[ReCl_4(NO)_2]$. In this latter case the reaction was predicted to be symmetry forbidden for d^5 or higher electron count [55]. Experimental evidence strongly suggests that for complexes of rhodium, palladium and cobalt containing two cis nitrosyls, one linear and one bent, only the rhodium complexes are capable of disproportionation of NO, yielding N_2 and O_2 [56].

In the field of surface science, adsorbed dinitrosyls have been detected for oxide-supported MoO_3 [32–34], CrO_3 supported on silica [37,35], Rh adsorbed on alumina [36], Rh exchanged into Y zeolites [38], Cu I exchanged into ZSM5 zeolites [41], evaporated nickel surfaces [57], as well as Pd(100) [27], Pd(111) [39] and Pt(111) surfaces [40,42]. However, an IR study using isotopic mixtures of NO suggests that the dimer interpretation is wrong in this latter case [28].

2. Goal

Starting from several adsorption geometries of linear NO, this study will concentrate on the formation of dinitrogen dioxide, N_2O_2, adsorbed on Rh, Pd and Pt surfaces. We shall focus on the strength of the N–N and N–O interactions to determine if this intermediate is a reasonable one in the reaction pathway leading to N_2 and O_2. Further, the dissociative versus molecular adsorption of nitrosyl on the above surfaces will be discussed.

3. Methodology

The simplest general picture of NO chemisorption in the linear form fits the Blyholder model [58] – electron donation from the 5σ-orbital into suitable transition-metal d orbitals and back-donation from the metal orbitals into the very low lying 2π orbitals which contain one electron. Both depopulation of the 5σ orbital and

population of the 2π orbitals contribute to form a strong M–N bond and weaken the N–O bond.

Closely related theoretical studies have shown that differences between various surface orientations of a given metal are smaller than those arising from changing the metal [59]. Therefore, we chose the (100) face of three fcc structures of rhodium, palladium and platinum, modeling the surfaces with a three-layer two-dimensional slab. The nearest-neighbor separation is 2.6893, 2.75 and 2.77 Å for rhodium, palladium and platinum respectively [60].

The analysis was carried out using the extended Hückel tight-binding methodology [61–66]. In order to trace the adsorbate–surface interactions, a fragment molecular orbital (FMO) analysis was performed using densities of states (DOS) and crystal orbital overlap population (COOP) and their decompositions [67]. Further computational details are listed in the appendix. The extended Hückel method is approximate, best at indicating trends in bonding and identifying the most important interactions.

Although the saturation coverage of NO on Rh(100) is 0.65 ML, this study used a hypothetical coverage of 1.0 ML for most starting geometries. Such a high coverage was dictated by computational economy. However, we have previously shown that both overlap populations and electron densities of the FMO's are mostly coverage independent [68], and we have also obtained similar results with a calculated coverage of 0.67. On the other hand, the binding energy of the substrate decreases with increasing coverage, but this is not relevant in the present study [59,68]. It should be pointed out that the bridging site preference for linear nitrosyls on Rh(100), deduced by comparing the different binding energies, has been demonstrated previously by this group [68]. The consequences of NO bending on this same surface [68] as well as on Ni(111) [69] have been studied in detail with the extended Hückel methodology.

4. Geometry

The geometry of the absorbed coupled dinitrogen dioxide was chosen so as to be able to observe changes in N–N overlap population. Rather than using 2.18 Å as reported in the crystal structure of dinitrogen dioxide [45], we set a N–N

Table 1
Bonding characteristics for on-top M(NO) and bridging $M(N_2O_2)$

	NO [c]	On-top Rh(NO)	On-top Pd(NO)	On-top Pt(NO)	Bridging $Rh(N_2O_2)$	Bridging $Pd(N_2O_2)$	Bridging $Pt(N_2O_2)$	N_2O_2 [d]
FMO occupation [a]								
$5\sigma^+$	2.00	1.74	1.76	1.70	1.89	1.90	1.89	2.00
$5\sigma^-$	2.00	1.72	1.78	1.68	1.61	1.55	1.43	2.00
$2\pi_y^-$	2.00	1.11	0.54	0.35	1.74	1.19	1.36	0.00
$2\pi_x^+$	0.00	1.05	0.44	0.32	1.79	0.31	0.48	2.00
$2\pi_x^-$	0.00	1.12	0.24	0.32	0.49	0.08	0.17	0.00
$2\pi_y^+$	0.00	1.06	0.13	0.28	0.03	0.02	0.03	0.00
Overlap population								
M–N		0.85	0.56	0.73	0.63	0.52	0.64	
N–N	0.00	0.00	0.00	0.00	0.72	0.61	0.62	0.61
N–O	1.13	0.87	1.24	1.23	0.80	1.06	1.03	0.95
ΔE [b]					1.41	1.08	1.12	0.68

[a] The FMO's are listed in order of decreasing energy for the starting geometry **1**. It should be noted that the same ordering leaves the $2\pi_x^+$ orbital formally empty in the coupled dinitrosyl of geometry **2**.

[b] Corresponds to the difference in energy (eV) between the coupled product bridging $M(N_2O_2)$ and the corresponding uncoupled geometry on-top M(NO) $\Delta E = E_{\text{bridging}}\ M(N_2O_2) - E_{\text{on-top}}\ M(NO)$.

[c] See geometry **1**.

[d] See geometry **2**.

bond length of 1.44 Å and a N–N–O angle of 120°. The reasons for this choice of distance, shorter than in the gas-phase N_2O_2, are: (i) the adsorbed N_2O_2, as we will show later, may have a stronger N–N bond, (ii) this adsorbed species should be regarded as an intermediate on the reaction pathway leading from NO to N_2, and (iii) both Casewit and Rappé [54] and we [55] have used such short distances in related molecular calculations (1.53 and 1.44 Å respectively). Both N–O bond length and M–N distances were kept constant for all calculations: 1.17 and 1.8 Å respectively. A molecular calculation was carried out for both starting geometry **1** and the coupled product **2**.

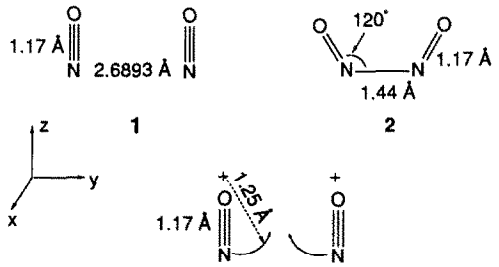

Computed FMO occupations and overlap populations are presented in table 1.

As an FMO analysis will be carried out, it is necessary to have a good picture of the fragment orbitals involved in the interaction between the substrate and the surface. We included two nitrosyls per unit cell, to have the same number of FMO's in the starting geometry as in the coupled product A Walsh diagram for the coupling reaction of two nitrosyls is presented in fig. 1. The reaction coordinate, sketched at the bottom of fig. 1, consists of an approach of the two N ends of the two NO's, the oxygen atoms barely moving in the same direction. For both geometries **1** and **2**, we introduce labels for the FMO's reminiscent of their origin, derived from 5σ and 2π orbitals. The two linear combinations of 5σ will be denoted $5\sigma^+$ and $5\sigma^-$ for the in- and out-of-phase combinations. Bringing the two nitrosyls together in the *yz* plane lifts the degeneracy of the $2\pi_x$ and $2\pi_y$ orbitals. Again, these orbitals form in- and out-of-phase combinations as the two nitrosyl molecules come into action. In the starting geometry, both nitrosyls lie parallel to each other at 2.6893 Å apart, corresponding to the nearest neighbor separation in Rh(100). At this distance, the splitting of the $5\sigma^+$ and $5\sigma^-$ and the $2\pi_x^+$ and $2\pi_x^-$ FMO's is barely noticeable. On the other hand, the $2\pi_y^-$ and $2\pi_y^+$ are split by 0.35 eV; the overlap of the $2\pi_y$ orbitals begins to be substantial at this separation.

As the nitrosyl molecules approach each other, the N–N bonding orbitals are stabilized. This is the case for the $5\sigma^+$, $2\pi_x^+$ and $2\pi_y^-$ orbitals. Conversely, the orbitals which bear N–N antibonding character are shifted up in energy as both nitrogen atoms approach each other. This reaction is symmetry forbidden for an electron count of 22, eleven electrons per nitrosyl (see fig. 1). However, the HOMO–LUMO gap is very small for both the pair of nitrosyls (geometry **1**) (0.15 eV) and the coupled dinitrogen dioxide geometry **2** (0.12 eV). The two-electron assignment in the $2\pi_y$ orbital ($2a_1$) in geometry **1** can therefore be regarded as arbitrary. From a ther-

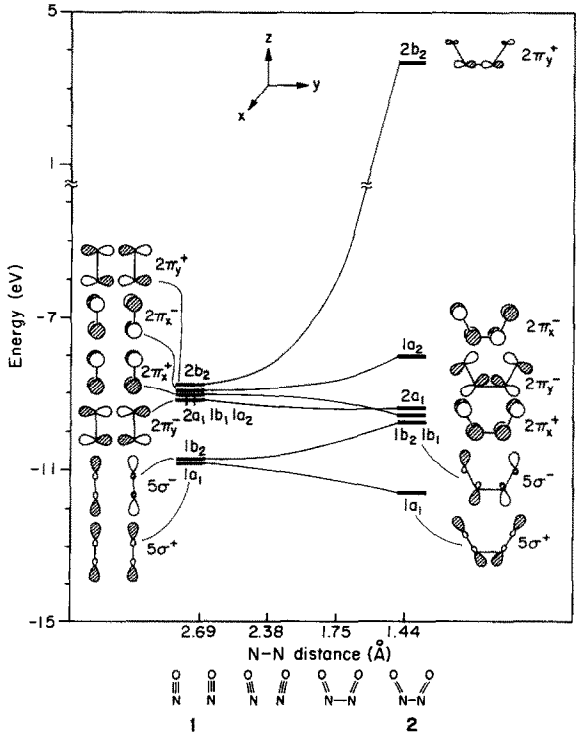

Fig. 1. Walsh diagram for the coupling of two NO molecules involving the formation of an N–N bond.

modynamic point of view, the coupled product **2** is disfavored by ~ 0.7 eV.

5. Monolayer of NO and N_2O_2

Moving to a monolayer of NO molecules, the molecular orbitals we saw above eventually grow into a band. With a square monolayer of nitrosyls having a cell constant of 2.6893 Å, these bands do pick up some dispersion (see fig. 2a), but the individual FMO's are still easily identifiable. The same applies to a square monolayer of dinitrogen dioxides with a cell constant of 3.8032 Å, resulting from a pairwise coupling of nitrosyl molecules as depicted in **2** (see fig. 2b).

6. Clean metal slabs

Let us now consider the clean metal surfaces. The calculated density of states for a three-layer rhodium slab shows a quite wide d band between −7.0 and −13.0 eV. The dispersed s and p bands lie mostly above the d band, with some penetration into it (fig. 3a). Moving on to a palladium

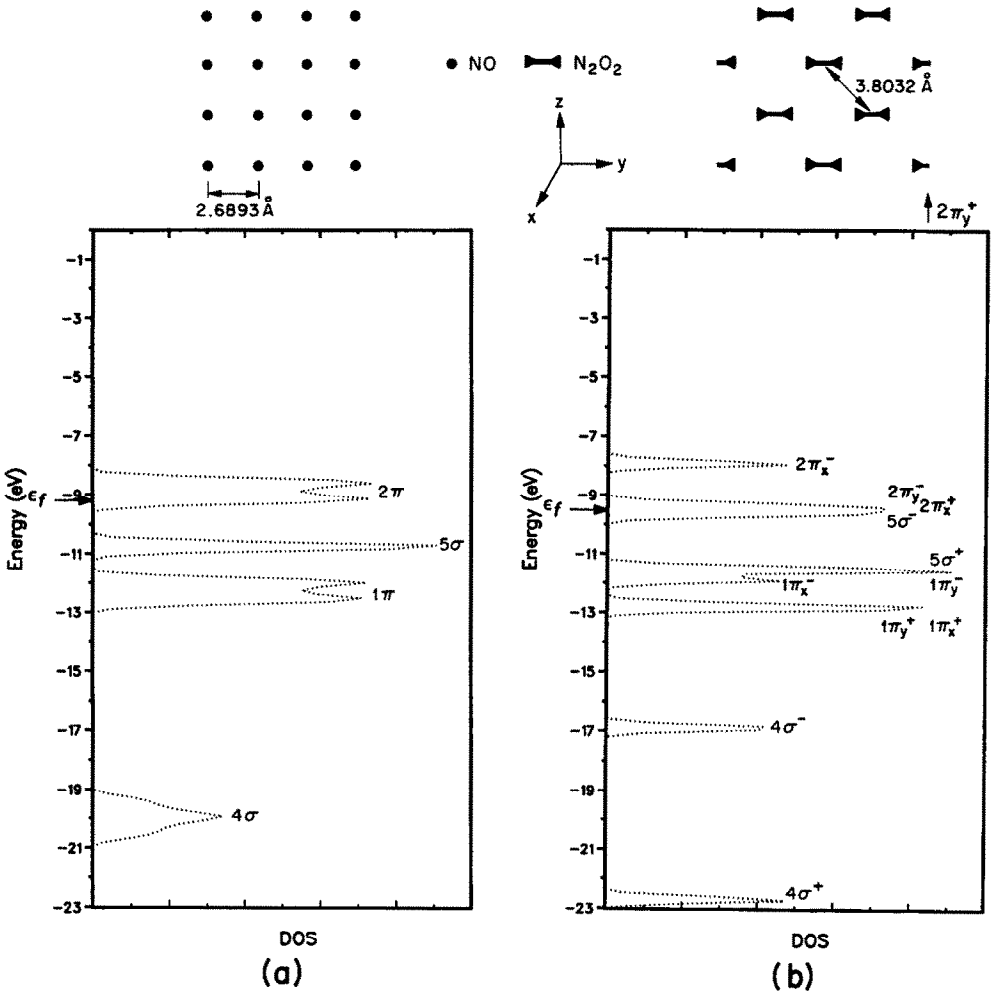

Fig. 2. (a) Total DOS of square NO monolayer with a 2.6893 Å separation. (b) Total DOS of N_2O_2 monolayer with a 3.8032 Å separation.

slab, fig. 3b, we see that the d band is significantly narrower, −11.0 to −13.0 eV. The platinum slab is intermediate with a d band width of 3.5 eV between −9.2 and −12.7 eV (fig. 3c). Whether the use of a three-layer slab model to represent the surface is appropriate has been discussed by this group in great detail earlier [59,68,69]. Because of the adsorbate's high coverage, we tried a five-layer slab in a couple of cases. The results were very similar with those obtained with a three-layer slab, which are consistently reported in this paper.

7. Interactions turned on

We now turn on the interaction between the adsorbates and the metal surfaces. The stabilization energy for an interaction goes as

$$\Delta E = \frac{|H_{ij}|^2}{E_i^0 - E_j^0}. \tag{1}$$

If the orbital energies dominate, as we think is the case for the three metal slabs, we can estimate the strengths of adsorbate–substrate interactions by focusing on the energy differences $E_i^0 - E_j^0$. This assumption was assessed with a molecular calculation. By varying the metal orbital exponents ξ while keeping the ionization potentials H_{ii} constant, we showed that the resonance integrals H_{ij} did not vary significantly. Thus, for identical geometries but different metal slabs, the energy term seems to dominate in the second-order perturbation expression (1).

Before studying specific adsorption geometries, one can qualitatively estimate the value of the denominator in eq. (1) by inspecting the dif-

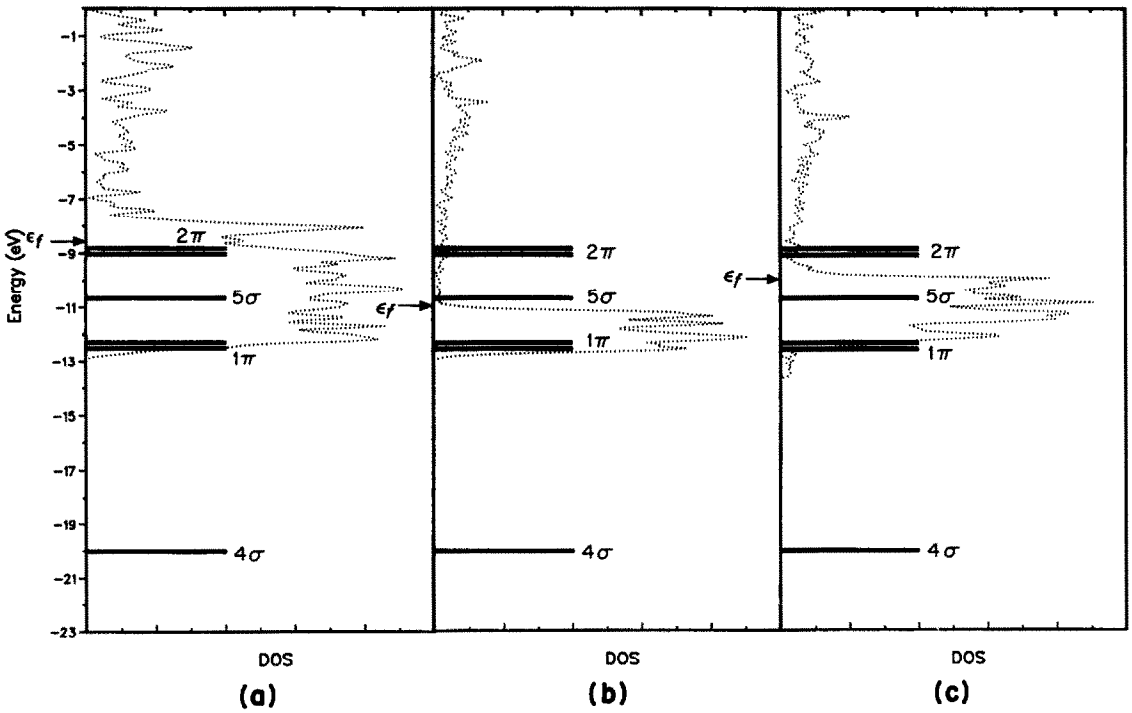

Fig. 3. Total DOS of a M(100) three layer slab. The straight lines correspond to the molecular orbitals of N_2O_2 (geometry 2): (a) M = Rh, (b) M = Pd, and (c) M = Pt.

ference in energy between the individual FMO's of the substrate and the clean metal surfaces. This is depicted in fig. 3 for the starting situation of vertical nitrosyls superimposed over a rhodium three-layer slab (fig. 3a), a palladium three-layer slab (fig. 3b), and a platinum three-layer slab (fig. 3c). The same process is repeated for the FMO's of N_2O_2 and the various metal slabs, figs. 4a, 4b and 4c, for rhodium, palladium and platinum respectively.

From fig. 3a, we predict a good interaction for all 5σ and 2π levels of NO adsorbed on Rh(100). As all these levels are all located "in the d band", a good interaction is expected. The palladium situation is quite different, fig. 3b. Since the d band is significantly narrower for palladium than for rhodium, the 2π levels are expected to interact only weakly with the d band. The 5σ levels lie at the top of the d band, and their interaction with the palladium slab is expected to be good. The platinum situation is intermediate between rhodium and palladium, fig. 3c. Again, the width of the d band allows prediction of the strength of interaction: the 5σ levels interact very strongly, whereas the 2π levels, lying slightly above the d band, should interact moderately with the platinum slab.

The same analysis can be carried out for the coupled product adsorbed on the various metal slabs, fig. 4. The $2\pi_y^+$ level is shifted up in energy to 3.68 eV upon coupling. Its interaction with either metal slab will be insignificant. For the rhodium slab, all other levels are expected to interact strongly with the metal surface, fig. 4a. Since for the palladium case only the $5\sigma^+$ level lies within the d band, no other level will interact very significantly with the slab, fig. 4b. Finally, for N_2O_2 adsorbed on platinum, except for the $2\pi_y^+$

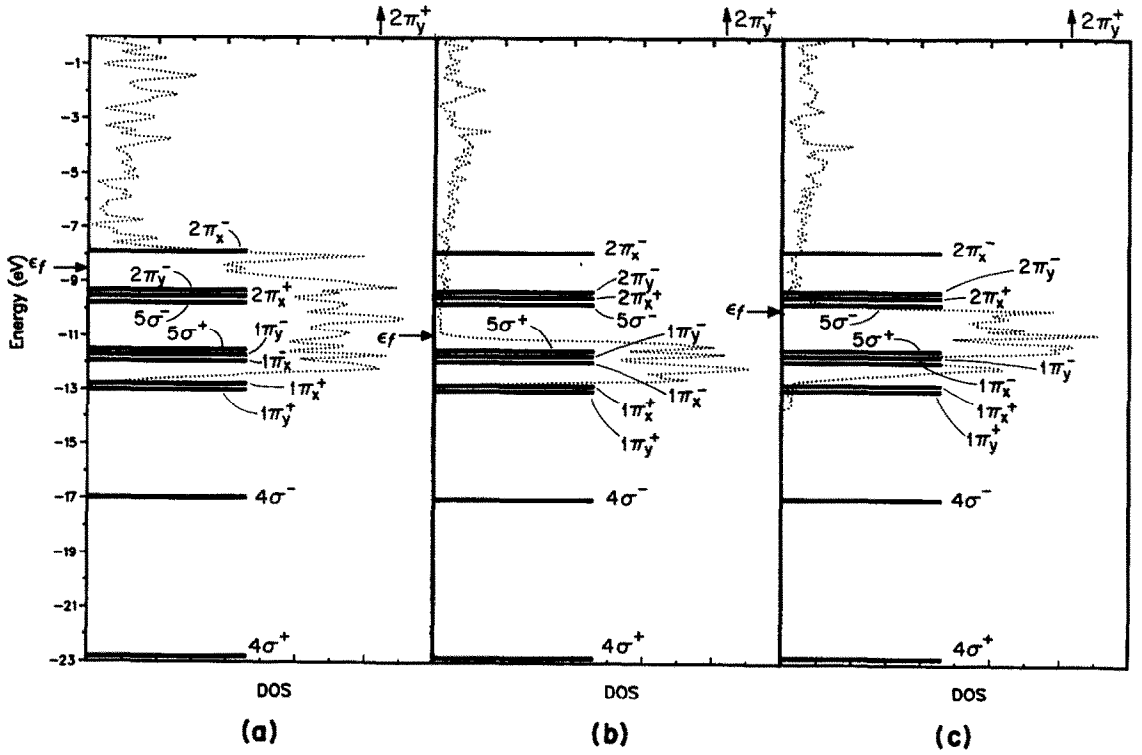

Fig. 4. Total DOS of a M(100) three layer slab. The straight lines correspond to the molecular orbitals of NO: (a) M = Rh, (b) M = Pd, and (c) M = Pt.

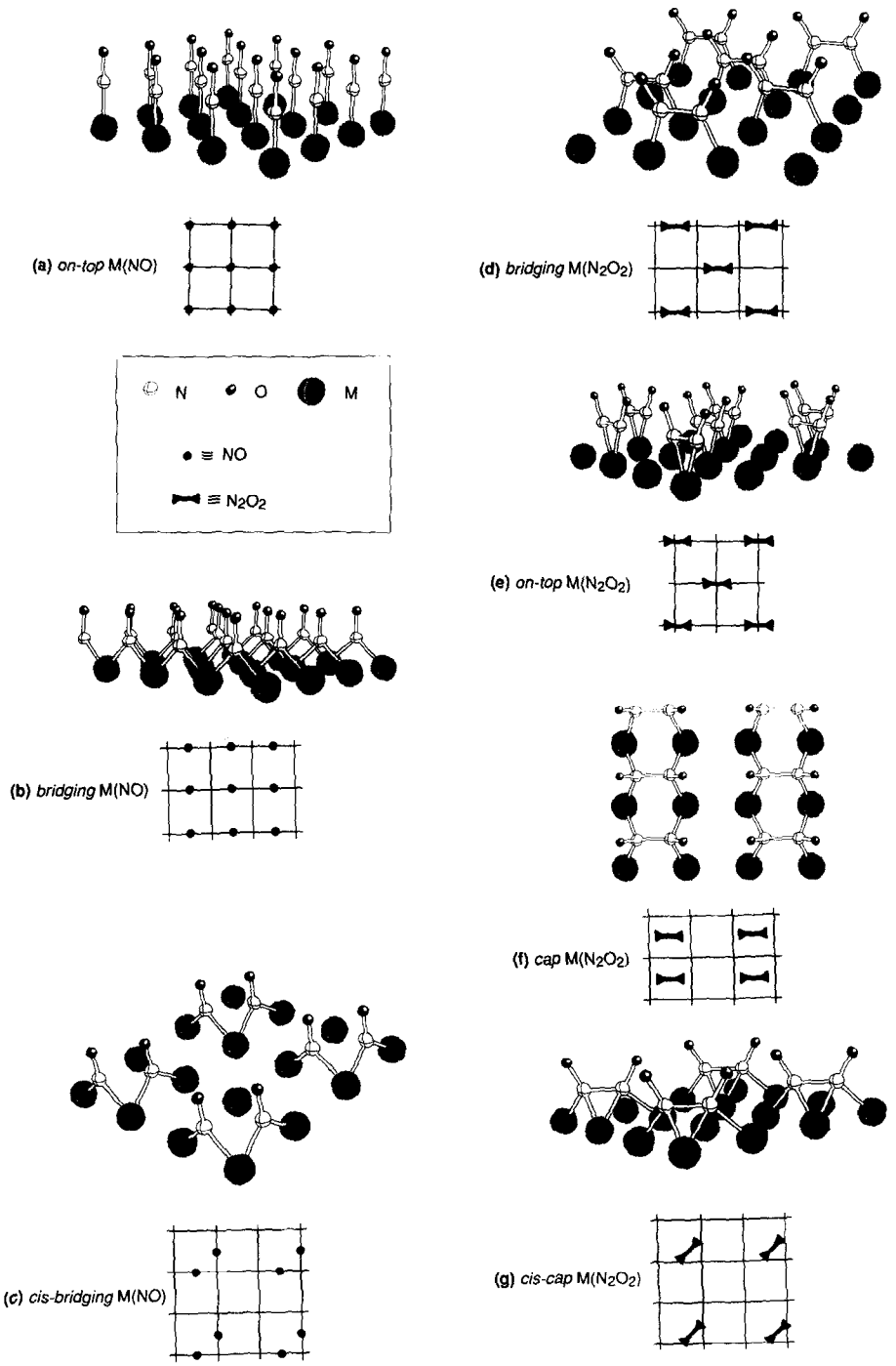

Fig. 5. (a) On-top M(NO). (b) Bridging M(NO). (c) Cis-bridging M(NO). (d) Bridging $M(N_2O_2)$. (e) On-top $M(N_2O_2)$. (f) Cap $M(N_2O_2)$. (g) Cis-cap $M(N_2O_2)$.

and $2\pi_x^-$, all other levels lie in the d band, and, therefore, their interaction with the metal slab is expected to be good (fig. 4c).

8. Specific adsorptions

Let us now turn to specific adsorption geometries for both substrates under study. Three starting coverages for linear nitrosyl adsorbed on M(100) surfaces of fcc metals were chosen: on-top p(1 × 1)NO + M(100) [referred to as on-top M(NO)] (fig. 5a), bridging p(1 × 1)NO + M(100) [bridging M(NO)] (fig. 5b), and cis-bridging (2 × 2)NO + M(100) [cis-bridging M(NO)] (fig. 5c). These geometries seem to cover the range of experimentally determined and conceptually reasonable adsorptions for a linear nitrosyl interacting with the (100) face of an fcc metal. The calculations were carried out with the three metal slabs (M = Rh, Pd, Pt). Keeping the metal–nitrogen (1.8 Å) and nitrogen–oxygen distances (1.17 Å) constant, the nitrosyl adsorbates were tilted pairwise to form dimers with a nitrogen–nitrogen distance of 1.44 Å and an N–N–O angle of 120°, as in **2**. From the on-top M(NO) situation, fig. 5a, by bending the nitrosyls pairwise towards each other, a bridging dinitrogen dioxide species is formed: bridging c(2 × 2)N_2O_2 + M(100) [bridging M(N_2O_2)] (fig. 5d). Two coupled geometries were studied starting from the bridging M(NO) situation, fig. 5b. In the first, two nitrosyls were tilted pairwise so as to have the oxygen–nitrogen vectors point towards a single metal atom, on-top c(2 × 2)N_2O_2 + M(100) [on-top M(N_2O_2)], fig. 5e. The second alternative involves the formation of a N_2O_2 unit embedded in the fourfold hollow of the fcc (100) surface: cap p(2 × 1)N_2O_2 + M(100) [cap M(N_2O_2)] (fig. 5f). Finally, starting from the cis-bridging M(NO) situation, fig. 5c, a coupling as depicted in fig. 5g was studied leading to cis-cap p(2 × 2)N_2O_2 + M(100) [cis-cap M(N_2O_2)]. It should be noted that a similar geometry was reported recently for an fcc Pd(100) surface [27].

By inspecting the various FMO's and the group orbitals of same symmetry on the surface, it is possible to estimate the relative magnitude of the overlap integrals and therefore the numerator of the perturbation theory expression (1).

8.1. On-top M(NO)

The local bonding interactions for both on-top M(NO) and bridging M(N_2O_2), the corresponding coupled product, are depicted in figs. 6a and b, respectively. Relevant electron densities of the substrate FMO's and overlap populations for both situations are summarized in table 1.

Let us analyze the on-top M(NO) situation first. As both 5σ and 2π levels are in resonance with the d band of the rhodium slab, the interaction is expected to be good. Indeed, both 5σ orbitals donate ~ 0.25 electrons upon interacting with the rhodium slab. Each 2π orbital hosts over 1.0 electron once the interaction is turned on. Since these four orbitals share two electrons before interaction with the slab, they have formally received ~ 0.5 electrons upon chemisorption. The on-top Rh(NO) thus fits nicely the Blyholder picture: σ-donation from the nitrosyl to

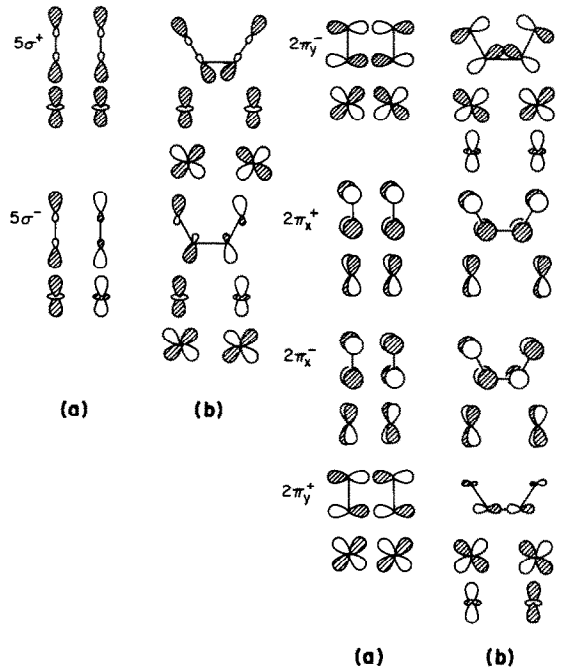

Fig. 6. (a) Relevant adsorbate–surface interactions for on-top M(NO). (b) Relevant adsorbate–surface interactions for bridging M(N_2O_2).

the surface and π-backbonding from the metal orbitals into the π^* orbitals of the adsorbate. The N–O bond is significantly weakened as a result: the overlap population is reduced from 1.13, computed for a pair of NO molecules (geometry **1**), to 0.87 for on-top Rh(NO) (see table 1). Both these interactions cooperate to form a strong Rh–N interaction; the corresponding overlap population is 0.85. Considering both these overlap populations, one could argue that the canonical structure M=N=O is more appropriate than M–N≡O for this chemisorption system. This qualitative conclusion is also based on some model calculations by us on discrete molecules. Although the coverage is at its maximum, no N–N bonding is in evidence.

The bonding picture changes dramatically with the palladium slab. The 5σ orbitals interact efficiently with the d band of the palladium slab; ~ 0.25 electrons are donated. As the 2π levels lie ~ 2 eV above the top of the d band, no backdonation from the metal slab to the adsorbate is observed. On the contrary, electrons are transferred to the metal. This is caused by the fact that part of the two electrons present in the antibonding 2π levels have been "dumped" into the d band at the Fermi level. A consequence is a relatively small Pd–N overlap population, 0.56, and a strengthening of the N–O bond. The corresponding overlap population increases from 1.13 in geometry **1** to 1.24 for on-top Pd(NO) (table 1).

The on-top Pt(NO) case follows closely the palladium situation. Again, in this case, the 2π levels of the free NO lie ~ 1 eV above the Fermi level and part of the electron density is transferred to the metal slab, resulting in a strengthening of the N–O bond upon interaction (table 1). To illustrate our point, the total DOS as well as the projected $2\pi_x^+$ FMO are depicted in figs. 7a, 7b and 7c for on-top M(NO), M=Rh, Pd and Pt respectively. For on-top Pd(NO) and on-top Pt(NO), since the N–O interaction is comparatively strong and the M–N interaction is weak, the M–N≡O representation is appropriate.

Clearly, the behavior of the N–O overlap population for the rhodium case differs dramatically from both other slabs. This observation alone accounts for the tendency of rhodium to cleave a

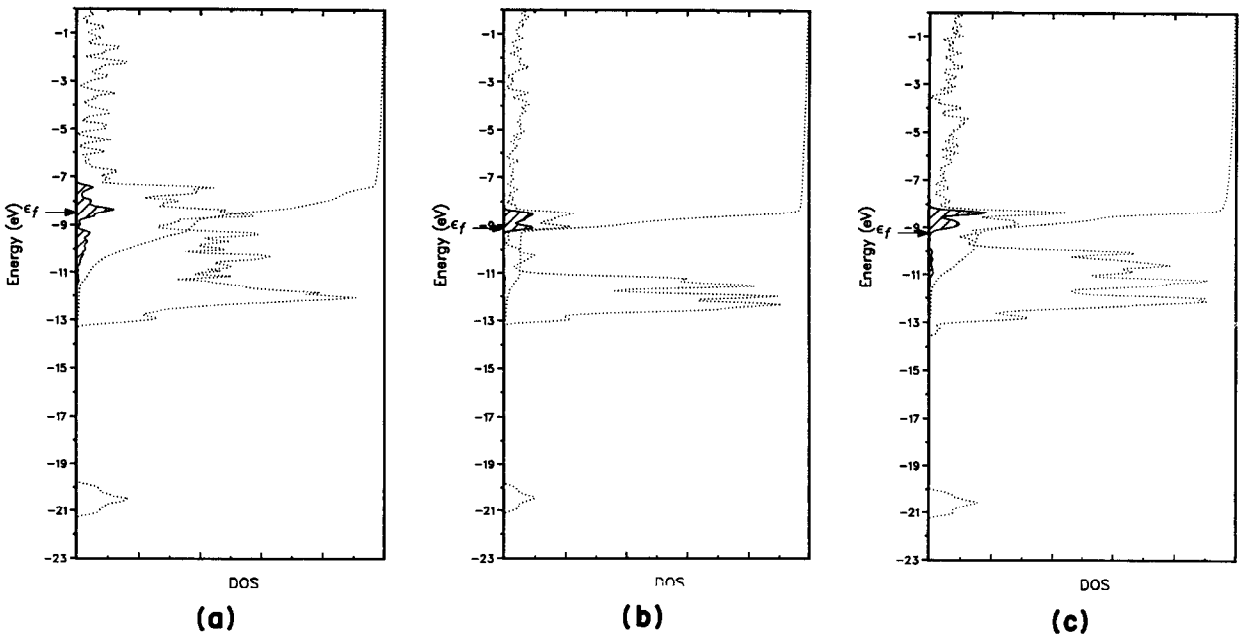

Fig. 7. Total DOS (dotted line) and the projected $2\pi_x^+$ FMO (striped area, magnified) for (a) on-top Rh(NO), (b) on-top Pd(NO), and (c) on-top Pt(NO).

nitrosyl into its atomic components. As we shall see, this trend is independent of adsorption geometry.

8.2. Bridging $M(N_2O_2)$

Having analyzed the on-top M(NO) interactions in detail, we move on to the corresponding coupled product, bridging $M(N_2O_2)$. The local adsorbate–surface interactions for this geometry are depicted in fig. 6b. These allow qualitative prediction of the magnitude of the overlap integrals responsible for bonding. Keeping in mind the energy terms dominating the perturbation expression (vide supra), the resulting electron occupations for the FMO's listed in table 1 come as no big surprise.

Comparing the overlap populations between the on-top M(NO) and the bridging $M(N_2O_2)$, we observe a significant N–N interaction, at the cost of both M–N and N–O interactions (see table 1).

As for the uncoupled case, both bridging $Pt(N_2O_2)$ and bridging $Pd(N_2O_2)$ have an increased N–O overlap population, 1.06 and 1.03 respectively, with respect to the free ligand of geometry **2** (0.95). On the other hand, for both bridging $Pt(N_2O_2)$ and bridging $Pd(N_2O_2)$, the N–N overlap population, 0.61 and 0.62 respectively, is close to the value for the free dinitrogen dioxide (geometry **2**, 0.61). The bridging $Rh(N_2O_2)$ situation differs quite dramatically; the N–N bond overlap population is 0.72, higher than that of free N_2O_2.

We can rationalize these overlap populations by looking at the FMO orbital occupations. The HOMO of the dinitrogen dioxide molecule corresponds to the $2\pi_x^+$ (see fig. 1). This orbital has a poor overlap with the slab, giving rise to a narrow projected DOS, which lies mostly above the Fermi level for both bridging $Pd(N_2O_2)$ and bridging $Pt(N_2O_2)$. The $2\pi_y^-$, which has a better overlap with the slab than $2\pi_x^+$, gets populated to various degrees. For both bridging Pd(NO) and bridging Pt(NO), $2\pi_x^-$ lies above the Fermi level before interaction. It picks up some bandwidth upon interaction and, eventually, levels are populated. Predictably, the $2\pi_y^-$ is most populated in bridging $Rh(N_2O_2)$. As both the $2\pi_x^+$ and $2\pi_y^-$ are strongly populated in the bridging $Rh(N_2O_2)$, by 1.79 and 1.74 electrons respectively, one could argue that the most appropriate description of the adsorbate is as a hyponitrite dianion with a 6π electron system. It should be noted that in this case both N–N and N–O overlap populations point towards a 6π electron system with a N–N double bond and a N–O single bond, as in hyponitrite (geometry **3**).

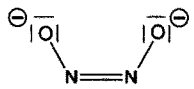

3

The computed N–N and N–O overlap populations for this 6π electron system are 0.80 and 0.62, respectively.

8.3. Other adsorption geometries of M(NO)

The rhodium slab clearly differs from both palladium and platinum ones in its ability either to cleave the adsorbed NO or to reduce the coupled product dinitrogen dioxide (geometry **2**) to hyponitrite (geometry **3**). We shall present the results for the other geometries by comparing their respective overlap populations.

Let us concentrate on the three starting geometries on-top M(NO), bridging M(NO) and cis-bridging M(NO), with M = Rh, Pt and Pt. Table 2 summarizes the overlap populations. To make it easier to compare the three slabs, we

Table 2
Overlap populations for M(NO)

	Overlap population	
	M–N	N–O
On-top Rh(NO)	0.85	0.87
Bridging Rh(NO)	0.61	0.85
Cis-bridging Rh(NO)	0.54 [a]	0.91
On-top Pd(NO)	0.56	1.24
Bridging Pd(NO)	0.44	1.16
Cis-bridging Pd(NO)	0.39 [a]	1.22
On-top Pt(NO)	0.73	1.23
Bridging Pt(NO)	0.57	1.06
Cis-bridging Pt(NO)	0.52 [a]	1.11

[a] Corresponds to the average overlap population for both unequivalent M–N bonds.

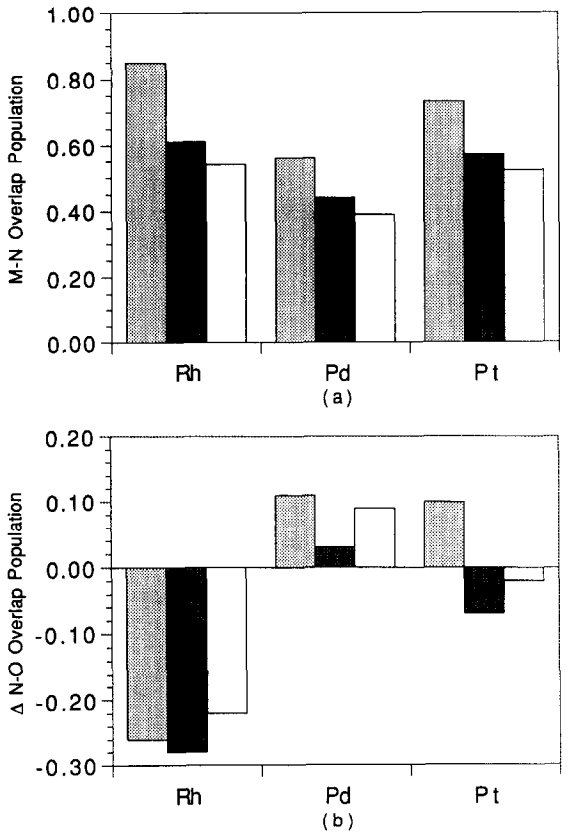

Fig. 8. Overlap population for three metal slabs and three adsorption geometries of NO. (a) M–N overlap population. (b) Difference in N–O overlap population N–O overlap population of a pair of NO molecules of geometry **1** and M(NO).

plotted the M–N and N–O overlap populations for the three metals and all the adsorption geometries on two graphs. In fig. 8a, the M–N overlap populations are presented for all three metal slabs with the three starting geometries. In fig. 8b, rather than plotting the N–O overlap population, we plotted the difference in overlap population between a pair of dinitrosyls (geometry **1**) and the N–O overlap population in the various adsorption geometries M(NO).

It is immediately apparent from fig. 8 that for all three starting geometries, on-top M(NO), bridging M(NO) and cis-bridging M(NO), the N–O overlap population is smallest for M=Rh. In all three geometries there is a significant amount of backbonding which contributes to destabilize the N–O bond when NO is adsorbed on Rh. Concerning the M–N overlap population, fig. 8b, the on-top M(NO) situation gives rise to the best interaction between either slab and the adsorbed NO. On-top Rh(NO) stands out clearly: a strong M–N overlap population coupled to a small N–O overlap population. However, in bridging Pt(NO) as well as cis-bridging Pt(NO), the N–O overlap population, 1.06 and 1.11, is lower than that of a pair of NO molecules of geometry **1** (1.13). This overlap population remains much greater than in the corresponding rhodium analogs, bridging Rh(NO) and cis-bridging Rh(NO) (0.85 and 0.91 respectively).

8.4. Other adsorption geometries of $M(N_2O_2)$

Let us turn now to the coupled product. Four geometries were considered (see figs. 5d–5g) and their respective M–N, N–O and N–N overlap populations are presented in table 3 and compared in figs. 9a, 9b and 9c respectively.

Table 3
Bonding characteristics for $M(N_2O_2)$

	Overlap population			ΔE [a]
	M–N	N–O	N–N	
Bridging $Rh(N_2O_2)$	0.63	0.80	0.72	1.41
On-top $Rh(N_2O_2)$	0.38	0.85	0.73	4.61
Cap $Rh(N_2O_2)$	0.43	0.79	0.79	4.40
Cis-cap $Rh(N_2O_2)$	0.34 [b]	0.81	0.65	1.88
Bridging $Pd(N_2O_2)$	0.52	1.06	0.61	1.08
On-top $Pd(N_2O_2)$	0.27	0.99	0.72	3.67
Cap $Pd(N_2O_2)$	0.36	1.02	0.57	2.40
Cis-bridging $Pd(N_2O_2)$	0.24 [b]	1.06	0.63	1.48
Bridging $Pt(N_2O_2)$	0.64	1.03	0.62	1.12
On-top $Pt(N_2O_2)$	0.39	1.04	0.64	4.42
Cap $Pt(N_2O_2)$	0.44	0.95	0.59	3.52
Cis-cap $Pt(N_2O_2)$	0.33 [b]	1.08	0.53	2.40

[a] Corresponds to the difference in energy (eV) between the coupled product $M(N_2O_2)$ and the corresponding uncoupled geometry M(NO) (see fig. 5) $\Delta E = E_{M(N_2O_2)} - E_{M(NO)}$.
[b] Corresponds to the average overlap population for both unequivalent M–N bonds.

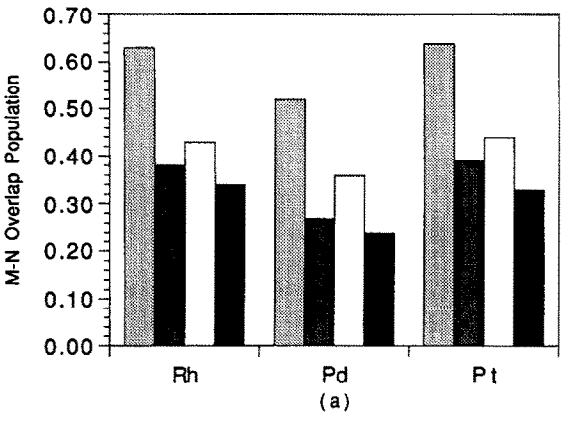

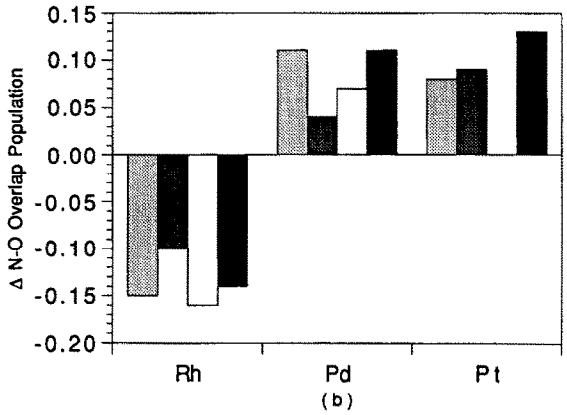

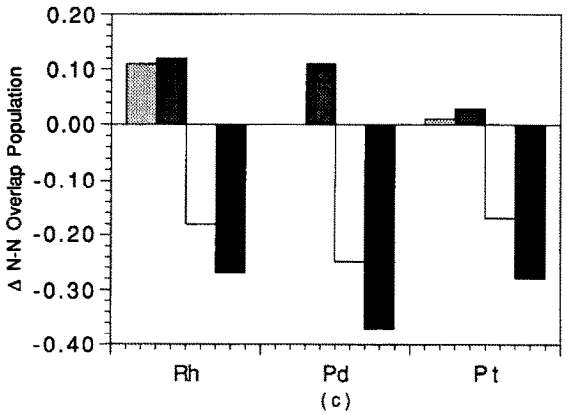

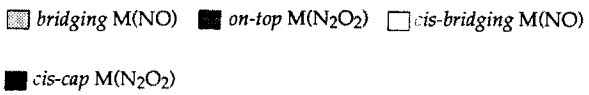

Fig. 9. Overlap populations for three metal slabs, M = Rh, Pd, Pt, and four adsorption geometries of N_2O_2 (geometry **2**). (a) M–N overlap population. (b) Difference in N–O overlap population between dinitrogen dioxyde and $M(N_2O_2)$. (c) Difference in N–N overlap population between dinitrogen dioxyde and $M(N_2O_2)$.

For all these geometries the N–O overlap population remains fairly constant as a function of the metal. This N–O overlap population is consistently smallest for N_2O_2 adsorbed on Rh, no matter what the adsorption geometry is (see fig. 9b). Further, it is smaller than the N–O overlap population of the free N_2O_2. For the other two slabs, palladium and platinum, the corresponding overlap population is generally greater than that in the free dinitrogen dioxide molecule, indicative of a strong N–O bond.

Looking at the N–N interaction, fig. 9c, we conclude that the overlap population is very much dependent on the adsorption geometry. It appears that both bridging $M(N_2O_2)$ and on-top $M(N_2O_2)$ situations give rise to a strong N–N interaction, and this regardless of the metal.

Finally, from a slab–adsorbate point of view, fig. 9a, the bridging $M(N_2O_2)$ situation gives rise to the strongest M–N interaction. It should be mentioned that all coupling reactions are unfavorable, from energetic considerations. The coupling path from on-top M(NO) to bridging $M(N_2O_2)$ seems to be most probable to us, since the differences in energy are smallest (see table 3). Total energies are not a strong point of extended Hückel calculations.

9. Conclusion

For all three adsorption geometries of NO on these metal slabs, we have shown by analyzing the N–O overlap population that the dissociative chemisorption is favored for rhodium surfaces. From our calculations, for both palladium and platinum slabs, it appears that the N–O bond is strengthened as the electron in the $2\pi^*$ orbital is dumped to the metal slab upon interaction.

We suggest that both on-top $M(N_2O_2)$ and bridging $Rh(N_2O_2)$ should have a strong N–N interaction, as well as a weakened NO interaction with respect to dinitrogen dioxide (geometry **2**), making them good candidates as intermediates in the rhodium-mediated reduction of NO. From an energetic point of view, only the coupling path from on-top Rh(NO) to bridging $Rh(N_2O_2)$ seems to be a reasonable route, one which could lead to

the formation of dinitrogen and oxygen from nitrosyls adsorbed on a rhodium surface.

We believe that it is mainly the width of the d band as well as the Fermi energy of the metal slab which determines the ability to couple pairs of nitrosyls, reducing them to a hyponitrite (geometry **3**). We are currently studying with the same methodology supported transition metals as well as various doping agents to explore the prospects of finding a substitute for rhodium in the TWC.

Acknowledgements

Our research was supported by a grant from the Ford Motor Company. TRW is thankful to the Swiss National Science Foundation for the award of a postdoctoral fellowship. We thank Ken Hass for many discussions and are grateful to Jane Jorgenson for her expert drawings.

Appendix

Tight-binding extended Hückel calculations, with a weighted H_{ij} approximation, have been applied throughout this paper. The H_{ii}'s for transition metals as well as nitrogen and oxygen were obtained from earlier work [68,70]. The Fermi energies for three-layer slabs computed with these values, using the extended Hückel methodology, are much larger than the experimental work functions of the metal slabs. It is our belief, however, that these rough computations give correct trends and electron shifts. Extended Hückel parameters for all atoms used are listed in table 4.

The geometrical assumptions concerning the bond lengths (in ångströms) used throughout this paper include the following: M–N 1.80, and NO 1.17 Å. The three-layer two-dimensional slab of the fcc metal structures used nearest neighbor separations of 2.6892 for rhodium, 2.75 for palladium and 2.76 Å for platinum [60].

A mesh of 64 $\boldsymbol{k}$ points was used in all calculations. To test the convergence, a mesh of 196 $\boldsymbol{k}$ points was used in several cases and no differences were observed. The $\boldsymbol{k}$ points were generated according to the geometrical method of Böhm and Ramirez [71].

Table 4
Extended Hückel parameters

Atom	Orbital	H_{ii} (eV)	ξ_1	ξ_2	c_1	c_2
N	2s	−23.95	1.95			
	2p	−10.95	1.95			
O	2s	−27.61	2.28			
	2p	−11.01	2.28			
Rh	5s	−7.31	2.13			
	5p	−3.39	2.10			
	4d	−10.35	4.29	1.97	0.5807	0.5685
Pd	5s	−7.24	2.19			
	5p	−3.68	2.15			
	4d	−11.90	5.98	2.61	0.55	0.67
Pt	6s	−9.15	2.55			
	6p	−4.38	2.55			
	5d	−11.00	6.01	2.70	0.63	0.55

References

[1] K.C. Taylor, Chemtech 20 (1990) 551.
[2] R.F. van Slooten and B.E. Nieuwenhuys, J. Catal. 122 (1990) 429.
[3] W.F. Egelhoff, Jr., in: Nitric Oxide Reduction, Vol. 4, Eds. D.A. King and D. P. Woodruff (Elsevier, Amsterdam, 1984) p. 390.
[4] G. Brodén, T.N. Rhodin, C. Bruckner, R. Benbow and Z. Hurych, Surf. Sci. 59 (1976) 593.
[5] R.J. Baird, R.C. Ku and P. Wynblatt, Surf. Sci. 97 (1980) 346.
[6] L.H. Dubois, P.K. Hansma and G.A. Somorjai, J. Catal. 65 (1980) 318.
[7] M.W. Leysley and L.D. Schmidt, Surf. Sci. 155 (1985) 215.
[8] H. Arai and H. Tominaga, J. Catal. 43 (1976)131.
[9] H. Conrad, G. Ertl, J. Küppers and E.E. Latta, Surf. Sci. 65 (1977) 235.
[10] A.A. Chin and A.T. Bell, J. Phys. Chem. 87 (1983) 3700.
[11] L.A. deLouise and N. Winograd, Surf. Sci. 154 (1985) 79.
[12] L.A. deLouise and N. Winograd, Surf. Sci. 159 (1985) 199.
[13] E. Ubach, S. Kulkarni, P. Feulner and D. Menzel, Surf. Sci. 88 (1979) 65.
[14] R. Hoffmann, M.M.-L. Chen, M. Elian, A.R. Rossi and D.M.P. Mingos, Inorg. Chem. 13 (1974) 2666.
[15] R. Eisenberg and C.D. Meyer, Acc. Chem. Res. 8 (1975) 26.

[16] J.H. Enemark and R.D. Feltham, Coord. Chem. Rev. 13 (1974) 339.
[17] R. Hoffmann, M.M.-L. Chen and D.L. Thorn, Inorg. Chem. 16 (1977) 503.
[18] G. Pirug, H.P. Bonzel, H. Hopster and H. Ibach, J. Chem. Phys. 71 (1979) 593.
[19] A.F. Carley, S. Rassias, M.W. Roberts and T.-H. Wang, Surf. Sci. 84 (1979) L227.
[20] S.C. Schwartz, G.B. Fisher and L.D. Schmidt, J. Phys. Chem. 92 (1988) 389.
[21] M. Bowker, Q. Guo and R.W. Joyner, Surf. Sci. 257 (1991) 33.
[22] H.P. Bonzel and G. Pirug, Surf. Sci. 62 (1977) 45.
[23] R.L. Klein, S.C. Schwarz and L.D. Schmidt, J. Phys. Chem. 89 (1985) 4908.
[24] R.J. Gorte and L.D. Schmidt, Surf. Sci. 111 (1981) 260.
[25] A. Obuchi, S. Naito, T. Onishi and K. Tamaru, Surf. Sci. 122 (1982) 235.
[26] S.W. Jorgenson, N.D.S. Canning and R.J. Madix, Surf. Sci. 179 (1987) 322.
[27] C. Nyberg and P. Uvdal, Surf. Sci. 204 (1988) 517.
[28] B.E. Hayden, Surf. Sci. 131 (1983) 419.
[29] M.E. Bartram, B.E. Koel and E.A. Carter, Surf. Sci. 219 (1989) 467.
[30] J.L. Gland and B.A. Sexton, Surf. Sci. 94 (1980) 355.
[31] J.S. Villarubia and W. Ho, J. Chem. Phys. 87 (1987) 750.
[32] H. Hattori, K. Tanabe, K. Tanaka and S. Okazaki, in: The Chemistry and Uses of Molybdenum, Proc. 3rd Int. Conference, Eds. H.F. Barry and P.C.H. Mitchell, Ann Arbor, MI, 1979, p. 188.
[33] H.C. Yao and W.G. Rothschild, in: The Chemistry and Uses of Molybdenum, Proc. 6rd Int. Conference, Eds. H.F. Barry and P.C.H. Mitchell, Ann Arbor, MI, 1982, p. 32.
[34] J. Valyon and W.K. Hall, J. Catal. 84 (1983) 216.
[35] E.L. Kugler, R.J. Kokes and J.W. Gryder, J. Catal. 36 (1975) 142.
[36] J. Liang, H.P. Wand and L.D. Spicer, J. Phys. Chem. 89 (1985) 5840.
[37] A. Zecchina, E. Garrone, C. Monterra and S. Coluccia, J. Phys. Chem. 79 (1975) 978.
[38] T. Iizuka and J.H. Lunsford, J. Mol. Catal. (1980) 391.
[39] H.-D. Schmick and H.-W. Wassmuth, Surf. Sci. 123 (1982) 471.
[40] M. Bertolo and K. Jacobi, Surf. Sci. 236 (1990) 143.
[41] G. Spoto, S. Bordiga, D. Scarano and A. Zecchina, Catal. Lett. 13 (1992) 39.
[42] H. Ibach and S. Lehwald, Surf. Sci. 76 (1978) 1.
[43] N.N. Greenwood and A. Earnshaw, Chemistry of the Elements (Pergamon, Oxford, 1984).
[44] M. Bodenstein, Helv. Chim. Acta 18 (1935) 745.
[45] W.N. Lipscomb and F.E. Wang, Acta Cryst. 14 (1961) 1100.
[46] C.E. Dinerman and G.E. Ewing, J. Chem. Phys. 53 (1970) 626.
[47] C.M. Western, P.R.R. Langridge-Smith and B.J. Howard, Mol. Phys. 44 (1981) 145.
[48] S. Skaarup, P.N. Skancke and J.E. Boggs, J. Am. Chem. Soc. 98 (1976) 6106.
[49] M.A. Benzel, C.E. Dykstra and M.A. Vincent, Chem. Phys. Lett. 78 (1981) 139.
[50] T.J. Lee, J.E. Rice, G.E. Scuseria and H.F. Schaefer, Theor. Chim. Acta 75 (1989) 81.
[51] R.D. Bardo, J. Phys. Chem. 86 (1982) 4658.
[52] B.F. Hoskins, F.D. Whillans, D.H. Dale and D.C. Hodgkin, Chem. Commun. (1969) 69.
[53] S. Bhaduri, B.F.G. Johnson, A. Pickard, P.R. Raithby, G.M. Sheldrick and C.I. Zuccaro, J. Chem. Soc. Chem. Commun. (1977) 354.
[54] C.J. Casewit and A.K. Rappé J. Catal. 89 (1984) 250.
[55] M. Kersting and R. Hoffmann, Inorganic Chem. 29 (1990) 279.
[56] W.R. Moser, in: The Catalytic Chemistry of Nitrogen Oxides, Eds. R.L. Klimisch and J.G. Larson (Plenum, New York, 1975) p. 33.
[57] M. Ito, T. Kato and W. Suĕtaka, Chem. Lett. (1976) 1337.
[58] G. Blyholder, J. Phys. Chem. 68 (1964) 2772.
[59] S.-S. Sung and R. Hoffmann, J. Am. Chem. Soc. 107 (1985) 578.
[60] J. Donahue, The Structure of the Elements (Krieger, New York, 1982).
[61] R. Hoffmann and W.N. Lipscomb, J. Chem. Phys. 37 (1962) 2872.
[62] R. Hoffmann and W.N. Lipscomb, J. Chem. Phys. 36 (1962) 2179.
[63] R. Hoffmann, J. Chem Phys. 39 (1963) 1397.
[64] J.H. Ammeter, H.-B. Bürgi, J.C. Thibeault and R. Hoffmann, J. Am. Chem. Soc. 100 (1978) 3686.
[65] M.-H. Whangbo and R. Hoffmann, J. Am. Chem. Soc. 100 (1978) 6093.
[66] M.-H. Whangbo, R. Hoffmann and R.B. Woodward, Proc. R. Soc. A 366 (1979) 23.
[67] R. Hoffmann, Solids and Surfaces: A Chemist's View of Bonding in Extented Structures (VCH Publisher, Weinheim, 1988).
[68] D.L. Vučković, S.A. Jansen and R. Hoffmann, Langmuir 6 (1990) 732.
[69] S.-S. Sung, R. Hoffmann and P.A. Thiel, J. Phys. Chem. 90 (1986) 1380.
[70] Y.-T. Wong and R. Hoffmann, J. Phys. Chem. 95 (1991) 859.
[71] R. Ramirez and M.C. Böhm, Int. Quantum Chem. 30 (1986) 391.